

Interlayer ferroelectric polarization modulated anomalous Hall effect in four-layer MnBi_2Te_4 antiferromagnets

Ziyu Niu,¹ Xiang-Long Yu,^{3,4} Dingfu Shao,⁵ Xixiang Jing,¹ Defeng Hou,¹ Xuhong Li,¹ Jing Sun,¹ Junqin Shi,^{1,2} Xiaoli Fan,^{1,2,*} and Tengfei Cao^{1,2,†}

¹Research Center for Advanced Lubrication and Sealing Materials, School of Materials Science and Engineering, Northwestern Polytechnical University, Xi'an, Shaanxi 710072, People's Republic of China

²State Key Laboratory of Solidification Processing, Northwestern Polytechnical University, Xi'an, Shaanxi 710072, People's Republic of China

³Shenzhen Institute for Quantum Science and Engineering, Southern University of Science and Technology, Shenzhen 518055, China

⁴International Quantum Academy, Shenzhen 518048, China

⁵Key Laboratory of Materials Physics, Institute of Solid State Physics, HFIPS, Chinese Academy of Sciences, Hefei 230031, China



(Received 5 January 2024; accepted 19 March 2024; published 2 May 2024)

Van der Waals (vdW) assembly could efficiently modulate the symmetry of two-dimensional (2D) materials that ultimately governs their physical properties. Of particular interest is the ferroelectric polarization being introduced by proper vdW assembly that enables the realization of novel electronic, magnetic, and transport properties of 2D materials. Four-layer bulklike stacking antiferromagnetic MnBi_2Te_4 (*FB*-MBT) offers an excellent platform to explore ferroelectric polarization effects on magnetic order and topological transport properties of nanomaterials. Here, by applying symmetry analyses and density-functional-theory calculations, the ferroelectric interface effects on magnetic order, anomalous Hall effect (AHE) or even quantum AHE (QAHE) on the *FB*-MBT are analyzed. Interlayer ferroelectric polarization in *FB*-MBT efficiently violates the $\hat{P}\hat{T}$ symmetry [the combination of central inversion (\hat{P}) and time reverse (\hat{T}) symmetry] of the *FB*-MBT by conferring magnetoelectric couplings, and stabilizes a specific antiferromagnetic order encompassing a ferromagnetic interface in the *FB*-MBT. We predict that engineering an interlayer polarization in the top or bottom interface of *FB*-MBT allows converting *FB*-MBT from a trivial insulator to a Chern insulator. The switching of ferroelectric polarization at the middle interfaces results in a direction reversal of the quantum anomalous Hall current. Additionally, the interlayer polarization of the top and bottom interfaces can be aligned in the same direction, and the switching of polarization direction also reverses the direction of anomalous Hall currents. Overall, our work highlights the occurrence of quantum-transport phenomena in 2D vdW four-layer antiferromagnets through vdW assembly. These phenomena are absent in the bulk or thin-film in bulklike stacking forms of MnBi_2Te_4 .

DOI: [10.1103/PhysRevB.109.174405](https://doi.org/10.1103/PhysRevB.109.174405)

I. INTRODUCTION

The manipulation of symmetry can yield distinct phases of matter and, thus, unique material properties [1]. The time-reversal symmetry (\hat{T}) breaking directly impacts spin polarizations and leads to the generation of spontaneous magnetic orders, forming the foundation for spintronic devices. Magnetic field, either an external or intrinsic one, can be applied to break the \hat{T} of the system and induces spin polarizations. However, large amounts of electric current are typically required to generate effective magnetic field, which could cause significant energy losses. Additionally, for fully compensated antiferromagnets, magnetic field cannot efficiently control their magnetic orders and poses significant limitations for applications of antiferromagnets in electronic devices [2–8].

It is anticipated that electric voltage-controlled magnetization could offer noteworthy benefits for nonvolatile, low-power spintronic devices [9,10]. On the occasion of the centenary of ferroelectricity discovery, Wu *et al.* predicted interlayer ferroelectricity for the first time in two-dimensional van der Waals (vdW) materials [11]. This theoretical breakthrough has the potential to significantly expand our understanding of ferroelectric properties and drive groundbreaking technological advancements in thin-film and multilayered nanostructured materials. Interlayer ferroelectricity has been confirmed by a series of vdW assembly experiments [12–18]. Ferroelectric polarization induced by interlayer stacking, even relatively weak ($\sim 0.01 \mu\text{C}/\text{cm}^2$) [19–21] compared with perovskites ($28.6 \mu\text{C}/\text{cm}^2$ for PbTiO_3) [22] or binary metal-oxide ($51.39 \mu\text{C}/\text{cm}^2$ for HfO_2) [23], enables novel electronic and transport properties that were previously unattainable in bulk materials or vdW films in bulklike stacking patterns [17,18,24–26]. It is because interlayer polarization could efficiently break intrinsic symmetries of crystals, and lifts symmetry restrictions on electronic properties of different

*xlfan@nwpu.edu.cn

†tengfei.cao@nwpu.edu.cn

crystals. For example, by introducing interlayer polarization, the $\hat{P}\hat{T}$ symmetry of the system is broken, which removes Kramers degeneracies of band structures and greatly impacts their electronic transport properties. Furthermore, the interlayer ferroelectricity generated through vdW assembly not only expands the range of ferroelectric materials but also provides an efficient means to explore novel properties that were previously unattainable in bulk materials or bulklike stacking films [18].

Among all two-dimensional (2D) vdW materials, the introduction of interlayer polarization into the antiferromagnetic topological family MB_2T_4 ($M = \text{Ti, V, Cr, Mn, Fe, Co, Ni, Eu}$; $B = \text{Bi, Sb}$; $T = \text{Te, Se}$) stands out as the most fascinating [27]. The magnetic, ferroelectric, and topological transport properties in MB_2T_4 family can potentially interact in interesting ways, leading to a direct impact on the occurrence of quantum phenomena such as anomalous Hall effect (AHE) or even quantum AHE (QAHE) [2].

MnBi_2Te_4 , serves as a prototype member of the MB_2T_4 family, which exhibits A-type antiferromagnetic order [4], and has been successfully synthesized in experiments [28]. The interaction between magnetic ordering and topological states can yield a range of quantum phenomena [29–32]. Specifically, the emergence of quantum states in MnBi_2Te_4 thin films is strictly dependent on its layer numbers N . When N is even, there is no detectable anomalous Hall conductance (AHC) and it is predicted to be an axion insulator [33,34]; when N is odd, it is able to show a plateau of quantum anomalous Hall conductance of e^2/h around the Fermi energy level, associating with QAHE [5]. The phenomenon can be explained in terms of different magnetic space group in even or odd layers of MnBi_2Te_4 .

Four-layer bulk-stacking MnBi_2Te_4 (FB - MBT) structures are special existing states of MnBi_2Te_4 thin films. On the one hand, they inherit the $\hat{P}\hat{T}$ symmetry of the parent bulk phase; On the other hand, they acquire surface structures that are not available in the bulk phases. Furthermore, compared with bilayer MnBi_2Te_4 with $\hat{P}\hat{T}$ symmetry, FB - MBT films possess three interlayer spaces allowing for introduction and alignment of interlayer polarization along different directions. This introduces various coupling effects among electric dipoles, magnetic orders, and topological states. Based on ideas that ferroelectric polarization breaks intrinsic symmetry of FB - MBT [20], we expect that the arranging of interlayer polarization at different locations will produce attractive physical correlations between ferroelectricity, magnetic order, topological transport properties, and surface states.

Here, by combining symmetry analysis and first-principles calculations, we show that interlayer ferroelectric polarization could efficiently induce AHE or even QAHE in FB - MBT films. Specifically, because of $\hat{P}\hat{T}$ symmetry breaking of the FB - MBT , nonzero AHC can always be obtained. Under the influence of interlayer ferroelectric polarization, it is possible to stabilize a unique antiferromagnetic order that includes a ferromagnetic interface and maintains a zero net magnetic moment. Our study demonstrates reversible quantized topological transport properties in magnetically fully compensated FB - MBT relying solely on the interlayer polarization, which has not been reported in previous work, and our predictions propose new avenues for efficiently controlling magnetic sym-

metry, consequently influencing spin-dependent topological transport properties, without the need for an external magnetic field.

II. METHODS

We perform all density functional theory (DFT) calculations by applying the Vienna *Ab initio* Simulation Package (VASP) [35]. The exchange and correlation effects are treated within the generalized gradient approximation (GGA) [36]. The GGA+U functional with $U_{\text{eff}} = 4$ eV on Mn 3d orbitals is applied in all calculations [37,38]. The value of U has been tested by Li *et al.* and for MnBi_2Te_4 , it was found that $U = 4$ eV provides the band structures that match well with the experiments [4]. Moreover, the $U = 4$ eV has been widely utilized in numerous theoretical studies to investigate the quantum transport properties of MnBi_2Te_4 [20,39,40]. The plane-wave energy cutoff is set to 500 eV in all calculations. A 15-Å vacuum region is used between adjacent plates to avoid the interaction between neighboring periodic images. The van der Waals (vdW) corrections, as parameterized within the semiempirical DFT-D3 method [41], are used in the calculations. The systems are fully relaxed until the residual force on each atom is less than 0.01 eV/Å. Electronic minimization is performed with a tolerance of 10^{-7} eV. Unless mentioned in the text, spin-orbit coupling (SOC) is always included in the calculations of the electronic and transport properties. The out-of-plane electric polarization of polar-stacked MnBi_2Te_4 films is calculated using the dipole correction method [42]. The maximally localized Wannier functions are used to obtain the tight-binding Hamiltonians within the WANNIER90 code [43]. The Berry curvature, the anomalous Hall conductivity, the surface band structure and the Chern number are calculated using the WANNIERTOOLS code [44].

III. RESULTS AND DISCUSSION

Figure 1(a) presents a four-layer bulklike stacked vdW magnetic MnBi_2Te_4 film (FB - MBT), where each MnBi_2Te_4 layer is composed of one MnTe layer and one Bi_2Te_3 layer, and the MnTe layer is embedded into Bi_2Te_3 matrix. Being similar to its parent bulk counterpart, the FB - MBT exhibits an out-of-plane A-type antiferromagnetic order [32] (Table S1 shows the relative energies of FB - MBT in different magnetic orders), and it also inherits the intrinsic $\hat{P}\hat{T}$ symmetry of the antiferromagnetic MnBi_2Te_4 bulk phase. Because of $\hat{P}\hat{T}$ symmetry restriction, there are no net magnetic moments in the FB - MBT , which prevents AHE that could be detected in the FB - MBT film. The $\hat{P}\hat{T}$ symmetry restriction on the AHE can be understood from the following intrinsic definition of the berry curvature ($\Omega(k)$) and anomalous Hall conductivity (σ_{xy}),

$$\Omega(k) = -2\text{Im} \sum_{m \neq n} \frac{\langle n | \frac{\partial \hat{H}}{\partial k_x} | m \rangle \langle m | \frac{\partial \hat{H}}{\partial k_y} | n \rangle}{(E_{nk} - E_{mk})^2}, \quad (1)$$

where \hat{H} is the Hamiltonian of the system, and E_{nk} is the energy of the n_{th} band at wave vector k . $|m\rangle$, $|n\rangle$ are corresponding eigenstates of \hat{H} . The intrinsic anomalous Hall conductivity (σ_{xy}) is calculated through the integration of

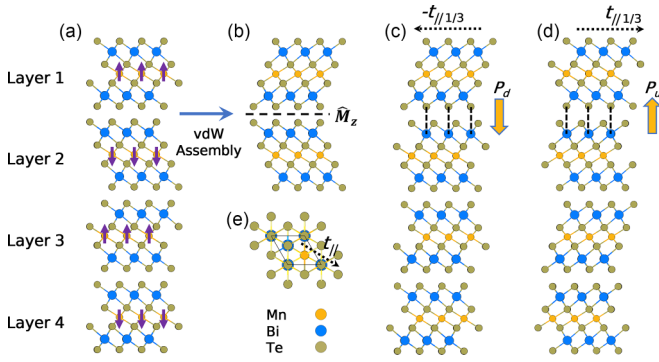


FIG. 1. (a), (e) Side and top views for atomic structures of *FB-MBT*. The purple arrows in (a) represent the direction of magnetic moments of Mn atoms. (b) A mirror-reflected (\hat{M}_z) bilayer structure was achieved by vdW assembly of layer1 and layer2 in the *FB-MBT* film without considering the bottom two-layers (a), leading to an unstable AA- stacking configuration. (c), (d) Schematic representation for the formation of a four-layered MBT film with an interlayer polarization P_d (c) or P_u (d) between layer1 and layer2 by sliding layer1 along the $-\mathbf{t}_{//1/3}$ or $\mathbf{t}_{//1/3}$ (e) direction within the plane from the AA stacking in (b).

$\Omega(k)$ in the whole Brillouin zone (BZ) [Eq. (2)]:

$$\sigma_{xy} = -\frac{e^2}{h} \int_{\text{BZ}} \frac{d^2\kappa}{2\pi} \Omega(k). \quad (2)$$

From the definition of $\Omega(k)$ in Eq. (1), it can be obtained that $\Omega(k)$ is an odd function under the $\hat{P}\hat{T}$ symmetry operation [$\hat{P}\hat{T}\Omega(k) = -\Omega(-k)$], which makes $\Omega(k)$ zero and the integration of $\Omega(k)$ in the whole BZ zero. Therefore, the AHE cannot be detected in the *FB-MBT*.

The $\hat{P}\hat{T}$ symmetry constraint on the AHE can be eliminated by manipulating the system's symmetry [39,45,46], with changing the stacking patterns of vdW materials being a method that can be explored through vdW assembly experiments [19,20]. Here, based on the *FB-MBT* [Fig. 1(a)], we show that $\hat{P}\hat{T}$ symmetry can be broken in four-layer MnBi_2Te_4 through introducing interlayer polarization. To simplify, the structure of a four-layer MnBi_2Te_4 is depicted in Fig. 1(a), with interlayer polarization being induced into the interlayer space between the top two layers. The interlayer atoms that generate out-of-plane ferroelectric polarization are highlighted.

In order to introduce interlayer polarization into this top two layers, we initially accomplished a 180° rotation of the top layer to break the inversion symmetry of the system. This rotational adjustment leads to the formation of top two-layer MnBi_2Te_4 film in AA stacking [Fig. 1(b)]. Furthermore, such noncentrosymmetric AA-stacked two-layer MnBi_2Te_4 film is unstable. The top MnBi_2Te_4 layer can spontaneously glide along the in-plane $\mathbf{t}_{//}$ [$1\bar{1}0$] or $-\mathbf{t}_{//}$ direction of the film, as indicated by the arrows in Fig. 1(e), to achieve the most stable electric polar structures. For clarity and improved readability, the term “*FP-MBT*” is used to refer to the four-layer MnBi_2Te_4 films with polar interfaces. The interlayer polarization in MnBi_2Te_4 is obtained with the Bi atoms in the bottom layer being aligned with the Te atoms in the top layer [Fig. 1(c)], or Bi atoms in the top layer being aligned with

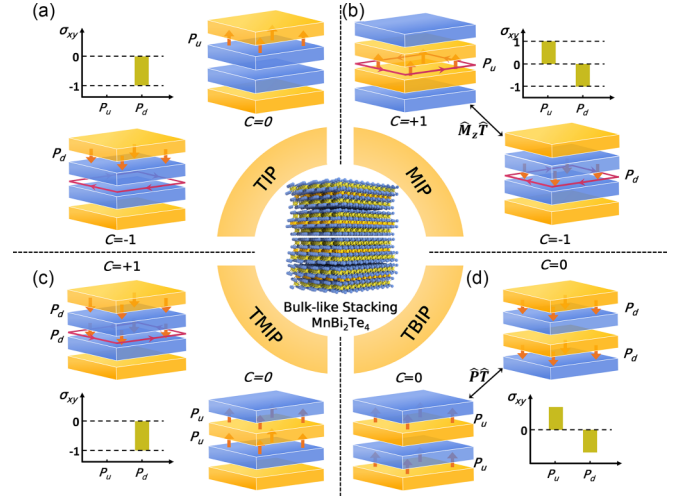


FIG. 2. (a) Bottom left and top right: schematic structure of polar stacked *TIP FP-MBT* with electric interlayer polarization directions in top interface of *FP-MBT* P_d and P_u , respectively. The yellow layer signifies that the magnetic moment of Mn atoms in the whole layer pointing up (\uparrow), and the blue one indicates that all magnetic moments point down (\downarrow). The orange arrows in the interlayer space represent the direction of electric polarization. Upper left: the AHC corresponding to the stacking pattern of the P_d and P_u at the Fermi energy level. (b) Bottom right and top left: the schematic diagram of the *MIP- P_d/P_u* stacking structure, where the electric interlayer polarization exists in the middle interfaces of the *FP-MBT*. Here the P_d and P_u states are connected by $\hat{M}_z\hat{T}$ symmetry [the combination of in-plane mirror (\hat{M}_z) and time reversal (\hat{T}) symmetry]. In the pattern of *MIP- P_d* , the Chern number is -1 and the Chern number is $+1$ for *MIP- P_u* , which is confirmed by the AHC at the Fermi energy level in the upper right corner. (c) Bottom right and top left: schematic conformation of a polarized *FP-MBT* films stacking mode between two adjacent interlayers with two identical orientations (*TMIP- P_u/P_d*), whose Chern numbers is 0 and 1, respectively, as confirmed by the AHC at the Fermi energy level (bottom left). (d) Bottom left and top right: Schematic representation of *TBIP- P_u/P_d* stacking models that retain the A-type antiferromagnetic order in the bulk phase and are associated by $\hat{P}\hat{T}$ symmetry operation. Schematic of the AHC at $E-E_f = 0.05$ eV, which implies that *TBIP- P_u/P_d* remain topologically trivial insulators in these stacking patterns. The specific atomic structures of all the stacking pattern mentioned above can be found in the Figs. 1(c) and 1(d) and in Supplemental Material [47] Fig. S1.

the Te atoms in the bottom layer [Fig. 1(d)]. Correspondingly, the direction of interlayer polarization points up (P_u) or down (P_d), respectively. For all *FP-MBT* films containing interlayer polarization, the original $\hat{P}\hat{T}$ symmetry of *FB-MBT* has been removed, which greatly impacts their magnetic ground states as well as the related topological transport properties.

We demonstrate that magnetic ground states and the AHE of *FP-MBT* are determined by interlayer polarizations, which are depicted schematically in Fig. 2. For *FP-MBT*, there are three interlayer positions where ferroelectric polarization can be introduced. To describe the polarization states between these different positions, we abbreviate the polarization between the top layer and second one as *TIP*, between the second and third layer as *MIP*, and between the bottom two layers as

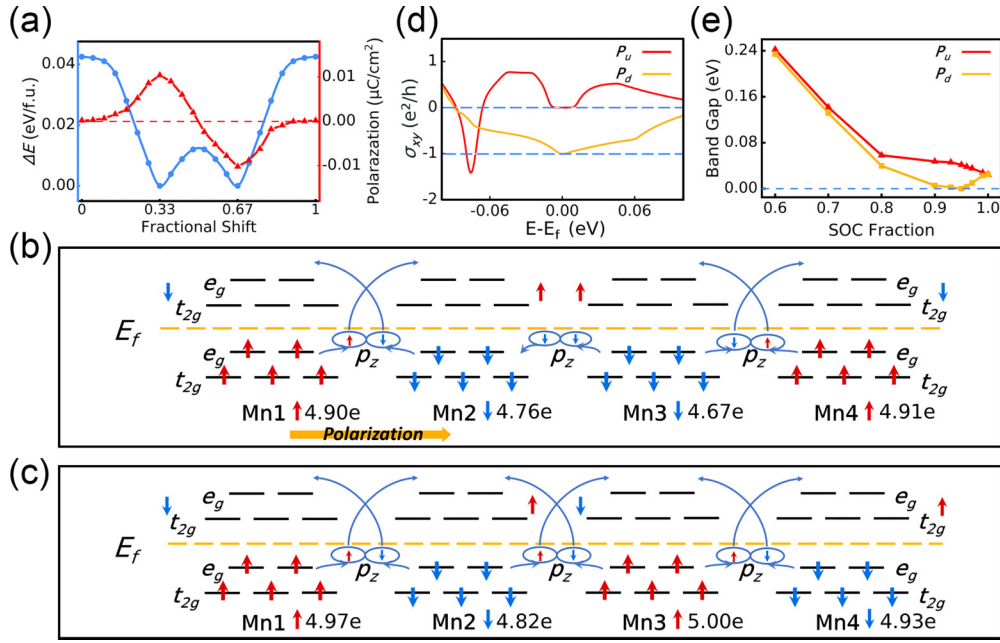


FIG. 3. (a) Total energy and out-of-plane electric polarization of a polar MnBi₂Te₄ bilayer when sliding the top monolayer with respect to the bottom along the [1 $\bar{1}$ 0] direction. The two minima in energy profile correspond to polarization in up P_u and down P_d direction. (b) The Schematic diagram of ferromagnetic coupling between Mn2 and Mn3 in four-layer MnBi₂Te₄ containing one interlayer polarization between Mn1 layer and Mn2 layer (FP -MBT). (c) The antiferromagnetic superexchange interactions for Mn atoms in FP -MBT film. In (b) and (c), the arrows denote the direction of spin polarization of Mn atoms. The light blue curves with an arrow denote hopping paths. (d) Anomalous Hall conductance σ_{xy} of TIP - P_d/P_u as a function of electron energy. (e) Variation of the band gap of TIP - P_d/P_u as a function of fractions of the actual SOC.

BIP. Similarly, the combination of two interlayer polarization is abbreviated as *TMIP* or *TBIP*, respectively, and the presence of polarization in all three interlayers is abbreviated as *AIP*. The polarization direction can point upwards or downwards; correspondingly, we denote them as *TIP*-, *MIP*-, *BIP*-, *TMIP*-, *TBIP*-, and *AIP*- $P_u(P_d)$.

We found that the magnetic ground state is closely connected to the interlayer polarizations in FP -MBT. For FB -MBT without interlayer polarization, the A -type up-down-down ($\uparrow\downarrow\downarrow$) magnetic order is the magnetic ground state. For TIP - P_u/P_d and MIP - P_u/P_d , our calculations show that the most stable magnetic order is ($\uparrow\downarrow\downarrow\uparrow$) [Figs. 2(a), 2(b), Tables S2, and S3]. For *TMIP* with two polar interfaces, the magnetic order could be ($\uparrow\downarrow\uparrow\downarrow$) or ($\uparrow\downarrow\downarrow\uparrow$) [Fig. 2(c), Table S4], depending on the direction of interlayer polarization, and for *TBIP* with two polar interfaces, the magnetic ground state is still A -type antiferromagnetic order ($\uparrow\downarrow\uparrow\downarrow$) (Table S6).

The topological transport properties of polar FP -MBT films are different from that of FB -MBT, which are directly determined by interlayer polarization and magnetic orders. Firstly, interlayer polarization has lifted the $\hat{P}\hat{T}\Omega(k) = -\Omega(k)$ symmetry constraint on the FB -MBT, and it results in a nonzero berry curvature and nonzero AHC in all FP -MBT films. Furthermore, we find that the ($\uparrow\downarrow\downarrow\uparrow$) magnetic order has the lowest energy in *TIP*, *TMIP*, and *MIP* [Figs. 2(a)–2(c), Tables S2–4] among all magnetic states. Finally, as it is schematically given in Figs. 2(a)–2(c), even the net magnetic moment for ($\uparrow\downarrow\downarrow\uparrow$) or ($\downarrow\uparrow\uparrow\downarrow$) magnetic order in four-layer MnBi₂Te₄ is still zero, the ferromagnetic coupling in the middle interface could also induce quantum anomalous

Hall conductivities (QAHC) in FP -MBT, being similar to MnBi₂Te₄ films having net magnetic moment. In the following paragraphs, we will specifically discuss interlayer polarization effects on magnetic order and topological transport properties of FP -MBT films.

Figure 3(a) shows one example of the energy profile and interlayer polarizations of FP -MBT system, where the top layer slides along the [1 $\bar{1}$ 0] direction with respect to bottom three bulklike stacked MnBi₂Te₄ films. The fractional value of $\mathbf{0}$ corresponds to the mirror-symmetric (\hat{M}_z) stacked layer1 and layer2 in FP -MBT. It is a high energy unstable stacking pattern. The structure at the fractional value of $\mathbf{1}$ is the same with that of $\mathbf{0}$, which indicates that the top layer has shifted the whole crystal periodicity of the system. The two energy minima appear at fraction of 0.33 and 0.66 of the whole sliding paths, corresponding to the structure of *TIP* with interlayer polarization pointing up (TIP - P_u), or down (TIP - P_d), respectively. In these structures, the Bi/Te or Te/Bi at the interface of layer1 or layer2 aligns along the out-of-plane Z direction, generating electronic dipole moment pointing from Te to Bi atoms. The calculated electric polarization is approximately $0.01\mu\text{C}/\text{cm}^2$, being almost the same to previous results on polarization stacking in bilayer MnBi₂Te₄ films [20].

According to the theory of exchange interaction in magnetic systems, superexchange interaction occurs when an intermediate nonmagnetic atom or ion mediates the exchange coupling between two magnetic ions. Here, intermediate nonmagnetic atoms are Te and Bi atoms, and magnetic ones are Mn atoms. The interlayer magnetic coupling occurs when indirect electron hopping between the d orbitals of a magnetic

element is mediated by connected p orbitals of Bi and Te atoms.

In each layer of MnBi_2Te_4 , the Mn atom is surrounded by Te atoms in a slightly distorted octahedral configuration. This configuration results in the splitting of d orbitals into a triple-generating t_{2g} state and a double-generating e_g state. In MnBi_2Te_4 bulk phase, or MnBi_2Te_4 films in bulklike stacking patterns, the electronic occupation number of each Mn atom is around $5e$ [Fig. 3(b)], and there are few charge transfers from d orbitals of Mn atom to its surrounding Te atoms, the e_g - p - e_g superexchange [Fig. 3(c)] interaction plays a dominant role in determining the interlayer magnetic coupling of MnBi_2Te_4 , and the interlayer magnetic order is antiferromagnetic one.

For FP -MBT films containing electronic interlayer polarizations [Fig. 3(b)], our results show that the d orbital occupation of Mn is efficiently modulated by the interlayer electric polarization. Here, we take TIP - P_d as an example and for clarification, the Mn atoms in four-layer MnBi_2Te_4 film from top layer to bottom one are labeled as Mn1, Mn2, Mn3, and Mn4, respectively. Our simulations show that their occupation numbers are 4.90e, 4.76e, 4.67e, and 4.91e, respectively. It indicates that, because of interlayer polarization, there are relatively large charge transfer from d orbitals of Mn atom to p orbitals of Te or Bi in middle two layers (the Mn2 layer and Mn3 layer) of FP -MBT, and at the same time the magnetic polarization is also partially forwarded from Mn to Te and Be atom in each corresponding layer. All these make the magnetic coupling between the Mn2 layer and Mn3 layer the ferromagnetic one [Fig. 3(b)]. In Fig. S5, we further calculated the energy difference between $\uparrow\downarrow\uparrow\downarrow$ and $\uparrow\downarrow\downarrow\uparrow$ order during the sliding process. It clearly shows that with the increasing interlayer polarization strength, the $\uparrow\downarrow\downarrow\uparrow$ magnetic order is gradually stabilized.

We further calculated the AHC [Fig. 3(d)] in TIP four films, and found that for both P_u and P_d TIP , they exhibit nonzero AHCs due to the breaking of $\hat{P}\hat{T}$ symmetry. However, there existed a noticeable distinction in the AHC around the Fermi level. Specifically, the P_d state displays a quantized anomalous Hall conductance plateau, but the P_u state shows a zero plateau. Moreover, the Chern number of the P_d state is calculated to be 1, but that of P_u is 0. All these prove that TIP - P_d state is a magnetic topological insulator, but TIP - P_u state is a trivial magnetic insulator. Furthermore, we have calculated the variation of the band gap with respect to the fractional strength of SOC. It can be observed in Fig. 3(e) and Fig. S2 that, for the TIP - P_u , its band gap gradually decreases with the increase of SOC strength, until it reaches the minimum bandgap of 24.5 meV at SOC fraction of 1. There is no energy band inversion here, and proves a trivial band structure. In contrast, for the TIP - P_d state, its band gap firstly decreases with increasing SOC strength, completely closes at $\text{SOC} = 0.95$ [red curve in Fig. 3(e), Fig. S3], and then the bandgap reopens and increases in width until it reaches 28.8 meV at $\text{SOC} = 1$. It proves that there is a band inversion in the energy band of TIP - P_d that possesses a nontrivial band structure, and produces quantized transport properties. The calculated berry curvatures for TIP - P_u and TIP - P_d are given in Figs. S4(a) and S4(b), which show that, for both P_u and P_d states, there is a sharp peak near the Γ point, while the berry curvature is nearly zero at other points. It indicates that the

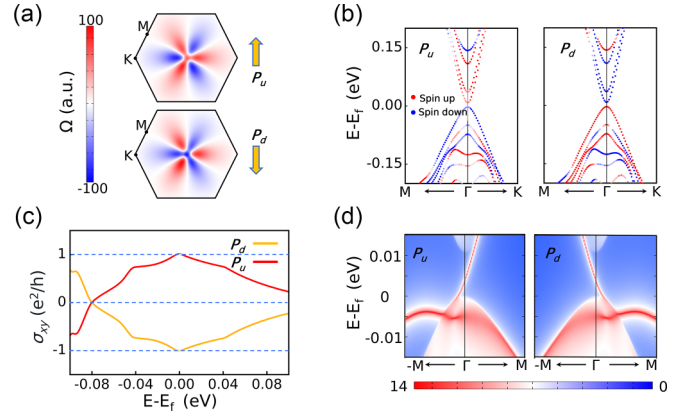


FIG. 4. (a) Berry curvature of the polar MIP FP -MBT in the 2D Brillouin zone calculated at the $E-E_f = 0.02$ eV for polarization pointing-up (top) and -down (bottom). (b) Energy bands near the Γ point of the MIP FP -MBT with P_u and P_d interface polarizations. The red region represents a dominant spin \uparrow configuration, while the blue area indicates a dominant spin-down one. (c) Anomalous Hall conductance σ_{xy} of the MIP FP -MBT as a function of electron energy for polarization P_u and P_d . (d) Surface band structures near the Γ point of the MIP FP -MBT film for P_u and P_d demonstrate the appearance of the topologically protected edge states at the Fermi level.

anomalous Hall conductivities in TIP are mainly contributed by the electronic states nearby the Γ point. Moreover, surface chiral edge state of TIP - P_d in Fig. S4(d) also clearly shows that there is one single surface state crossing the bandgap at the Γ point, which is consistent with the fact that TIP - P_d is a Chern insulator with Chern number equal to 1. For TIP - P_u [Fig. S4(c)], on the other hand, there are no chiral surface states could be observed and indicates normal semiconductor characters.

Apart from the TIP , we further analyze interlayer polarization effects on the MIP , where the interlayer polarization is induced between layer2 and layer3 [Figs. S1(a) and S1(b)]. Being similar to TIP , the MIP could also have interlayer polarization pointing-up (P_u) or -down (P_d), and these two states can be switched by crossing an energy barrier of 0.01 eV/f.u. The breaking of $\hat{P}\hat{T}$ symmetry in the MIP also leads to nonzero Berry curvature as well as nonzero anomalous Hall conductivities. The calculated Berry curvatures in the 2D BZ for P_u and P_d states of MIP are given in Fig. 4(a). It shows that, for both P_u and P_d polar states of MIP , the Berry curvature exhibits floral patterns, where the petals exhibit an alternating arrangement of red (positive value) and blue (negative value) colors. Moreover, the symmetry analysis for MIP indicates that the P_u and P_d are connected by $\hat{M}_z\hat{T}$ symmetry. Under $\hat{M}_z\hat{T}$ symmetry, the berry curvature of P_u state ($\Omega_u(k)$) and that of P_d state ($\Omega_d(k)$) is connected by the $\hat{M}_z\hat{T}\Omega_u(k) = -\Omega_d(-k)$ symmetry relation. It ensures that the color of each petal (reflecting the sign of $\Omega(k)$) remains independent of polarization. However, at the Γ point where $k = -k$, as the polarization direction changes from upward to downward, the Berry curvature $\Omega(k)$ also changes from positive value (isosurface color in red) to negative one (color in blue). Based on the nonzero Berry curvature, we calculated

the AHC for MIP in P_u and P_d states. Our results revealed a quantized plateau for both P_u and P_d state around the Fermi level with $\sigma_{xy} = \pm e^2/h$, which signifies the presence of quantum AHC (QAHC) in MIP state [Fig. 4(c)]. Furthermore, QAHC exhibits opposite sign when the ferroelectric polarization changes from the P_u state and the P_d one. The presence of QAHC is associated with nontrivial topological features of the system, as evidenced by the topologically protected edge states shown in Fig. 4(d). From the figure, it can be observed that the edge states of P_u and P_d exhibit chiral symmetry, indicating not only the presence of nontrivial topology in both systems but also the symmetry correlations between them. We also considered the electronic band structures for upward and downward polarization in the Fig. 4(b). When considering the SOC, the red or blue represents dominance of spin-up or spin-down states in the band structure, respectively, with the spin directions being unable to be accurately distinguished.

Due to $\hat{M}_z \hat{T} E^\uparrow(k) = E^\downarrow(-k)$, the reversal of spin characteristics with polarization direction, the colors of the bands are opposite. Moreover, FP -MBT with polarization stacking exhibits magnetoelectric multiferroicity, possessing both spontaneous polarization and ferromagnetic orders. Importantly, the QAHE is achieved with nearly zero uncompensated net magnetic moment (approximately 0.003 $\mu\text{B}/\text{f.u.}$), and it holds significant implications for enabling quantum devices resilient to external interference in the future.

FP -MBT has three interlayer spaces, each capable of exhibiting interlayer polarization. Electric polarizations in different interlayer spaces can either accumulate or nullify each other. Firstly, we analyze the accumulation effects of interlayer polarizations on magnetic ground states and topological transport properties of FP -MBT. One interlayer polarization exists between layer1 and layer2, and the other one exists between layer2 and layer3 (see atomic structure in Fig. S1). Both of them point in the same direction, either up or down, and they are named $TMIP$ - P_uP_u or $TMIP$ - P_dP_d , respectively. Based on calculations of different magnetic orders, we find that $TMIP$ - P_uP_u still maintains the bulklike A -type antiferromagnetic order ($\uparrow\downarrow\uparrow\downarrow$). For the $TMIP$ - P_dP_d states, the magnetic ground state is ($\uparrow\downarrow\downarrow\uparrow$), even the net magnetic moment is zero, there is ferromagnetic coupling between layer2 and layer3. These distinct magnetic orders indicate dissimilar magnetic transport properties of FP -MBT. We have calculated the AHC for both the upward and downward polarized structures [Fig. 5(c)]. In both cases, due to the breaking of $\hat{P}\hat{T}$ symmetry, the AHC above or below the band gap is nonzero. For the $TMIP$ - P_dP_d state, there is a quantized $\sigma_{xy} = e^2/h$ plateau near the Fermi level (red curve) in the AHC curve, indicating a topological insulator with the Chern number equal to 1, this is well supported by our calculations on the surface states in Fig. 5(d). Conversely, within the band gap region of the $TMIP$ - P_uP_u structure, the AHC curve is zero (yellow curve) and the calculated Chern number is 0 proving a trivial insulator.

The AHC curves of $TMIP$ - P_uP_u , $TMIP$ - P_dP_d in the vicinity of the Fermi level exhibit different widths of zero plateau or the quantized $\sigma_{xy} = e^2/h$ plateau, reflecting different band edge bending effects. We further analyzed the layer-dependent density of states (DOS) demonstrated in Figs. 5(a) and 5(b) to understand different interlayer polarization effects on band

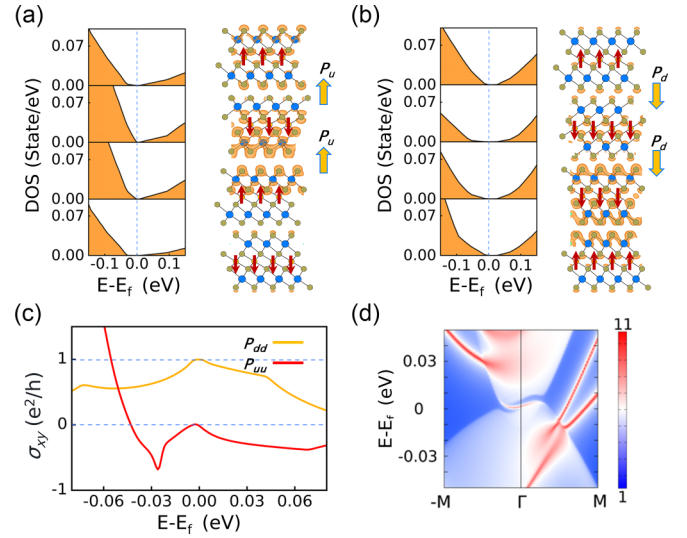


FIG. 5. FP -MBT film with interlayer polarizations in the top and middle interfaces ($TMIP$) and having polarization directions pointing-up $TMIP$ - P_u (a) and pointing-down $TMIP$ - P_d (b), and the corresponding layer-resolved density of states (DOS) as a function of energy (right). The real-space distributions of the charge density at the conduction band minimum are shown by brown colored isosurfaces of 0.8% of their maxima. (c) Anomalous Hall conductivity as a function of electron energy for $TMIP$ - P_uP_u and $-P_dP_d$. (d) Surface band structure of the $TMIP$ - P_dP_d indicates the appearance of the topologically protected edge states at the Fermi level.

gap of FP -MBT. Our analysis revealed that the band gap of $TMIP$ - P_uP_u is formed by the conduction band minimum (CBM) locating at layer2 or layer3 and valence band maximum (VBM) at layer2. For the $TMIP$ - P_dP_d state, the width of the band gap is determined by the VBM at layer1 or layer4 and the CBM locates at layer3. Moreover, it can be observed in Figs. 5(a) and 5(b) that the band gap is mainly determined by the position of the CBM, because the energy levels of the VBM are almost the same for the $TMIP$ - P_uP_u and the P_dP_d state. For the $TMIP$ - P_uP_u state, the charge predominantly resides within layer2 and layer3, which are more proximate to the polarization interface. The interlayer polarization could exert a significant influence on the band edge of the CBM, resulting in a smaller band gap. For the $TMIP$ - P_dP_d state, on the other hand, the CBM primarily localizes within layer3 and layer4, which has comparatively larger distance from the polarization interface than the case of $TMIP$ - P_uP_u , consequently, the effect of polarization on the band edge is attenuated, and the band gap of P_dP_d is relatively large.

Apart from the two nearest-neighbor polar interfaces mentioned above, we also analyze two polar interfaces that are separated by a nonpolar interface. One of these polar interfaces exists within layer1 and layer2, while the other one locates between layer3 and layer4. The polarization of the two interfaces points along the same direction, either up or down, and it is named $TBIP$ - P_uP_u , $TBIP$ - P_dP_d , respectively. This is a nonpolar interface between top and bottom electric polar interface. These polar structures could be achieved through contemporarily sliding layer1 and layer4 along the $\mathbf{t}_{//}$ or $-\mathbf{t}_{//}$

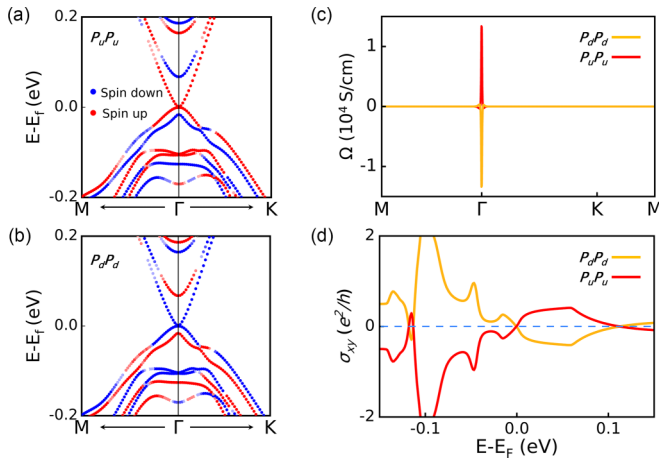


FIG. 6. (a), (b) Energy bands of the *FP*-*MBT* films with interlayer electric polarization in both top and bottom interface and the pointing-up (*TBIP*- $P_u P_u$) (a) or -down (*TBIP*- $P_d P_d$) (b). The red region represents dominating spin-up energy bands, while the blue region represents the spin-down one. (c) Berry curvature of the *TBIP*- $P_u P_u$ / $-P_d P_d$ along the high symmetric directions at Fermi energy. (d) Anomalous Hall conductivity as a function of electron energy for *TBIP*- $P_u P_u$ and $-P_d P_d$.

direction. Our calculations show that for both *TBIP*- $P_u P_u$ and *TBIP*- $P_d P_d$ state, they maintain *A*-type antiferromagnetic order of the bulklike four-layer $MnBi_2Te_4$ film. Our symmetry analysis shows that, even for each structure, the $\hat{P}\hat{T}$ has been broken because of the interlayer polarization, there is a $\hat{P}\hat{T}$ symmetry correlation between *TBIP*- $P_u P_u$ and *TBIP*- $P_d P_d$ polar structures. We can clearly see from Figs. 6(a) and 6(b) that with the reversal of the interlayer polarization direction, the spin states that dominate in the energy bands undergo a shift, which is manifested as a change in the color of the corresponding position. These symmetry relations also result in distinctive topological transport properties between *TBIP*- $P_u P_u$ and *TBIP*- $P_d P_d$. The results in Fig. 6(c) clearly shows that, the broken of $\hat{P}\hat{T}$ symmetry in either *TBIP*- $P_u P_u$ or *TBIP*- $P_d P_d$ leads to the nonvanishing Berry curvature, the peak is approximately $\pm 1.2 \times 10^4$ S/cm at the Γ point. Moreover, the sign of the Berry curvature is totally reversed with the reversal of the polarization direction because of the $\hat{P}\hat{T}$ symmetry connection [$\hat{P}\hat{T}\Omega(k) = -\Omega(k)$]. Furthermore, the calculated AHC (σ_{xy}) in Fig. 6(d) clearly show that, because of the $\hat{P}\hat{T}$ symmetry relation between *TBIP*- $P_u P_u$ and $-P_d P_d$

states, the direction of AHC in *TBIP* is totally determined by the direction of interlayer polarization. In the end, we also analyze four-layer $MnBi_2Te_4$ film with three polarization interfaces (*AIP*- P_u , *AIP*- P_d), the specific atomic structure is shown in Fig. S6, the higher polarization acts strongly on the bending of the band edges, leading to the closure of bandgap in both *AIP*- P_u and *AIP*- P_d , and finally only AHC is expected in fully polar structures. Tengfei Cao also thanks the support from the Youth Project of Shanxi High-level Talents Introduction Plan.

IV. SUMMARY

We have successfully implemented switchable interlayer polarization in $MnBi_2Te_4$ films with a four-layer van der Waals structure. Based on symmetry analysis and topological transport property calculations, we proposed that anomalous Hall effect (AHE), and even quantum anomalous Hall effect (QAHE) could be efficiently induced and modulated by interlayer polarization in four-layer *MBT*. The polar interface in four-layer $MnBi_2Te_4$ introduces a polarization-locked magnetic order. The generation of a ferromagnetic interface and breaking of the intrinsic $\hat{P}\hat{T}$ symmetry in four-layer $MnBi_2Te_4$ collectively induce novel topological transport properties that cannot be realized in the bulk state. Switching the polarization at the top or bottom interfaces has the capability to induce and modify the AHE and QAHE in a four-layer $MnBi_2Te_4$. Switching the polarization at the middle interfaces results in a reversal of the direction of the quantum anomalous Hall current. In addition, the interlayer polarization at the top and bottom interfaces may be oriented in the same direction, and reversing the polarization direction results in a reversal of the anomalous Hall current. These diverse quantum states, which are determined by interlayer polarization, can be readily achieved in experiments using vdW assembly. The investigation of various quantum states in $MnBi_2Te_4$ significantly enhances its potential applications in electronic and spintronic devices.

ACKNOWLEDGMENTS

This work is supported by the Fundamental Research Funds for the Central Universities (G2023KY05102), Natural Science Basic Research Program of Shaanxi (Program No. 2024JC-YBMS-009), and the Science and Technology on Reactor System Design Technology Laboratory. T.C. also thanks the support from the Youth Project of “Shanxi High-level Talents Introduction Plan.”

[1] L. J. Du, T. Hasan, A. Castellanos-Gomez, G. B. Liu, Y. G. Yao, C. N. Lau, and Z. P. Sun, Engineering symmetry breaking in 2D layered materials, *Nat. Rev. Phys.* **3**, 193 (2021).
 [2] C. Z. Chang, J. S. Zhang, X. Feng, J. Shen, Z. C. Zhang, M. H. Guo, K. Li, Y. B. Ou, P. Wei, L. L. Wang *et al.*, Experimental observation of the quantum anomalous Hall effect in a magnetic topological insulator, *Science* **340**, 167 (2013).
 [3] T. Taniguchi, Magnetoresistance generated from charge-spin conversion by anomalous Hall effect in metallic ferromagnetic/nonmagnetic bilayers, *Phys. Rev. B* **94**, 174440 (2016).

[4] J. H. Li, Y. Li, S. Q. Du, Z. Wang, B. L. Gu, S. C. Zhang, K. He, W. H. Duan, and Y. Xu, Intrinsic magnetic topological insulators in van der Waals layered $MnBi_2Te_4$ -family materials, *Sci. Adv.* **5**, eaaw5685 (2019).
 [5] Y. J. Deng, Y. J. Yu, M. Z. Shi, Z. X. Guo, Z. H. Xu, J. Wang, X. H. Chen, and Y. B. Zhang, Quantum anomalous Hall effect in intrinsic magnetic topological insulator $MnBi_2Te_4$, *Science* **367**, 895 (2020).
 [6] L. Smejkal, R. González-Hernández, T. Jungwirth, and J. Sinova, Crystal time-reversal symmetry breaking and

- spontaneous Hall effect in collinear antiferromagnets, *Sci. Adv.* **6**, eaaz8809 (2020).
- [7] T. Nan, C. X. Quintela, J. Irwin, G. Gurung, D. F. Shao, J. Gibbons, N. Campbell, K. Song, S. Y. Choi, L. Guo *et al.*, Controlling spin current polarization through noncollinear antiferromagnetism, *Nat. Commun.* **11**, 4671 (2020).
- [8] G. Gurung, D. F. Shao, and E. Y. Tsymlal, Transport spin polarization of noncollinear antiferromagnetic antiperovskites, *Phys. Rev. Mater.* **5**, 124411 (2021).
- [9] Z. Wang, T. Y. Zhang, M. Ding, B. J. Dong, Y. X. Li, M. L. Chen, X. X. Li, J. Q. Huang, H. W. Wang, X. T. Zhao *et al.*, Electric-field control of magnetism in a few-layered van der Waals ferromagnetic semiconductor, *Nat. Nanotechnol.* **13**, 554 (2018).
- [10] J. Q. Cai, D. Ovchinnikov, Z. Y. Fei, M. H. He, T. C. Song, Z. Lin, C. Wang, D. Cobden, J. H. Chu, Y. T. Cui *et al.*, Electric control of a canted-antiferromagnetic Chern insulator, *Nat. Commun.* **13**, 1668 (2022).
- [11] L. Li and M. H. Wu, Binary compound bilayer and multilayer with vertical polarizations: Two-dimensional ferroelectrics, multiferroics, and nanogenerators, *ACS Nano* **11**, 6382 (2017).
- [12] F. R. Sui, M. Jin, Y. Y. Zhang, R. J. Qi, Y. N. Wu, R. Huang, F. Y. Yue, and J. H. Chu, Sliding ferroelectricity in van der Waals layered γ -InSe semiconductor, *Nat. Commun.* **14**, 36 (2023).
- [13] P. Meng, Y. Z. Wu, R. J. Bian, E. Pan, B. Dong, X. X. Zhao, J. G. Chen, L. S. Wu, Y. Q. Sun, Q. D. Fu *et al.*, Sliding induced multiple polarization states in two-dimensional ferroelectrics, *Nat. Commun.* **13**, 7696 (2022).
- [14] S. Deb, W. Cao, N. Raab, K. Watanabe, T. Taniguchi, M. Goldstein, L. Kronik, M. Urbakh, O. Hod, and M. Ben Shalom, Cumulative polarization in conductive interfacial ferroelectrics, *Nature (London)* **612**, 465 (2022).
- [15] Z. Y. Fei, W. J. Zhao, T. A. Palomaki, B. S. Sun, M. K. Miller, Z. Y. Zhao, J. Q. Yan, X. D. Xu, and D. H. Cobden, Ferroelectric switching of a two-dimensional metal, *Nature (London)* **560**, 336 (2018).
- [16] Q. Yang, M. H. Wu, and J. Li, Origin of two-dimensional vertical ferroelectricity in WTe₂ bilayer and multilayer, *J. Phys. Chem. Lett.* **9**, 7160 (2018).
- [17] K. Yasuda, X. R. Wang, K. Watanabe, T. Taniguchi, and P. Jarillo-Herrero, Stacking-engineered ferroelectricity in bilayer boron nitride, *Science* **372**, 1458 (2021).
- [18] M. V. Stern, Y. Waschitz, W. Cao, I. Nevo, K. Watanabe, T. Taniguchi, E. Sela, M. Urbakh, O. Hod, and M. Ben Shalom, Interfacial ferroelectricity by van der Waals sliding, *Science* **372**, 1462 (2021).
- [19] R. Peng, T. Zhang, Z. L. He, Q. Wu, Y. Dai, B. B. Huang, and Y. D. Ma, Intrinsic layer-polarized anomalous Hall effect in bilayer MnBi₂Te₄, *Phys. Rev. B* **107**, 085411 (2023).
- [20] T. F. Cao, D. F. Shao, K. Huang, G. Gurung, and E. Y. Tsymlal, Switchable anomalous Hall effects in polar-stacked 2D antiferromagnet MnBi₂Te₄, *Nano. Lett.* **23**, 3781 (2023).
- [21] T. Zhang, X. Xu, B. Huang, Y. Dai, and Y. Ma, 2D spontaneous valley polarization from inversion symmetric single-layer lattices, *NPJ Comput. Mater.* **8**, 64 (2022).
- [22] O. Dahl, J. K. Grepstad, and T. Tybell, Polarization direction and stability in ferroelectric lead titanate thin films, *J. Appl. Phys.* **106**, 084104 (2009).
- [23] T. F. Cao, G. D. Ren, D. F. Shao, E. Y. Tsymlal, and R. Mishra, Stabilizing polar phases in binary metal oxides by hole doping, *Phys. Rev. Mater.* **7**, 044412 (2023).
- [24] Z. Y. Hao, A. M. Zimmerman, P. Ledwith, E. Khalaf, D. H. Najafabadi, K. Watanabe, T. Taniguchi, A. Vishwanath, and P. Kim, Electric field-tunable superconductivity in alternating-twist magic-angle trilayer graphene, *Science* **371**, 1133 (2021).
- [25] Y. R. Zhang, R. Polski, C. Lewandowski, A. Thomson, Y. Peng, Y. Choi, H. Kim, K. Watanabe, T. Taniguchi, J. Alicea *et al.*, Promotion of superconductivity in magic-angle graphene multilayers, *Science* **377**, 1538 (2022).
- [26] X. R. Wang, K. Yasuda, Y. Zhang, S. Liu, K. Watanabe, T. Taniguchi, J. Hone, L. Fu, and P. Jarillo-Herrero, Interfacial ferroelectricity in rhombohedral-stacked bilayer transition metal dichalcogenides, *Nat. Nanotechnol.* **17**, 367 (2022).
- [27] K. He, MnBi₂Te₄-family intrinsic magnetic topological materials, *npj Quantum Mater.* **5**, 90 (2020).
- [28] Y. Gong, J. W. Guo, J. H. Li, K. J. Zhu, M. H. Liao, X. Z. Liu, Q. H. Zhang, L. Gu, L. Tang X. Feng *et al.*, Experimental realization of an intrinsic magnetic topological insulator, *Chin. Phys. Lett.* **36**, 076801 (2019).
- [29] M. M. Otrokov, Klimovskikh II, H. Bentmann, D. Estyunin, A. Zeugner, Z. S. Aliev, S. Gass, A. U. B. Wolter, A. V. Koroleva, A. M. Shikin *et al.*, Prediction and observation of an antiferromagnetic topological insulator, *Nature (London)* **576**, 416 (2019).
- [30] C. Liu, Y. C. Wang, H. Li, Y. Wu, Y. X. Li, J. H. Li, K. He, Y. Xu, J. S. Zhang, and Y. Y. Wang, Robust axion insulator and Chern insulator phases in a two-dimensional antiferromagnetic topological insulator, *Nat. Mater.* **19**, 522 (2020).
- [31] A. Y. Gao, Y. F. Liu, C. W. Hu, J. X. Qiu, C. Tzschaschel, B. Ghosh, S. C. Ho, D. Bérubé, R. Chen, H. P. Sun *et al.*, Layer Hall effect in a 2D topological axion antiferromagnet, *Nature (London)* **595**, 521 (2021).
- [32] M. M. Otrokov, I. P. Rusinov, M. Blanco-Rey, M. Hoffmann, A. Y. Vyazovskaya, S. V. Ereemeev, A. Ernst, P. M. Echenique, A. Arnau, and E. V. Chulkov, Unique thickness-dependent properties of the van der Waals interlayer antiferromagnet MnBi₂Te₄ films, *Phys. Rev. Lett.* **122**, 107202 (2019).
- [33] W. Y. Lin, Y. Feng, Y. C. Wang, J. J. Zhu, Z. C. Lian, H. Y. Zhang, H. Li, Y. Wu, C. Liu, Y. H. Wang *et al.*, Direct visualization of edge state in even-layer MnBi₂Te₄ at zero magnetic field, *Nat. Commun.* **13**, 7714 (2022).
- [34] D. Q. Zhang, M. J. Shi, T. S. Zhu, D. Y. Xing, H. J. Zhang, and J. Wang, Topological axion states in the magnetic insulator MnBi₂Te₄ with the quantized magnetoelectric effect, *Phys. Rev. Lett.* **122**, 206401 (2019).
- [35] G. Kresse and J. Furthmüller, Efficient iterative schemes for *ab initio* total-energy calculations using a plane-wave basis set, *Phys. Rev. B* **54**, 11169 (1996).
- [36] J. P. Perdew, K. Burke, and M. Ernzerhof, Generalized gradient approximation made simple, *Phys. Rev. Lett.* **77**, 3865 (1996).
- [37] V. I. Anisimov, J. Zaanen, and O. K. Andersen, Band theory and mott insulators - Hubbard-U instead of stoner-I, *Phys. Rev. B* **44**, 943 (1991).
- [38] S. L. Dudarev, G. A. Botton, S. Y. Savrasov, C. J. Humphreys, and A. P. Sutton, Electron-energy-loss spectra and the structural stability of nickel oxide: An LSDA+U study, *Phys. Rev. B* **57**, 1505 (1998).

- [39] D. F. Shao, J. Ding, G. Gurung, S. H. Zhang, and E. Y. Tsymbal, Interfacial crystal Hall effect reversible by ferroelectric polarization, *Phys. Rev. Appl.* **15**, 024057 (2021).
- [40] P. Li, J. Y. Yu, Y. Wang, and W. D. Luo, Electronic structure and topological phases of the magnetic layered materials MnBi_2Te_4 , MnBi_2Se_4 , and MnSb_2Te_4 , *Phys. Rev. B* **103**, 155118 (2021).
- [41] S. Grimme, J. Antony, S. Ehrlich, and H. Krieg, A consistent and accurate *ab initio* parametrization of density functional dispersion correction (DFT-D) for the 94 elements H-Pu, *J. Chem. Phys.* **132**, 154104 (2010).
- [42] J. Neugebauer and M. Scheffler, Adsorbate-substrate and adsorbate-adsorbate interactions of Na and K adlayers on Al(111), *Phys. Rev. B* **46**, 16067 (1992).
- [43] G. Pizzi, V. Vitale, R. Arita, S. Blügel, F. Freimuth, G. Géranton, M. Gibertini, D. Gresch, C. Johnson, T. Koretsune *et al.*, Wannier90 as a community code: New features and applications, *J. Phys.: Condens. Mater.* **32**, 165902 (2020).
- [44] Q. S. Wu, S. N. Zhang, H. F. Song, M. Troyer, and A. A. Soluyanov, WannierTools: An open-source software package for novel topological materials, *Comput. Phys. Commun.* **224**, 405 (2018).
- [45] C. W. Niu, H. Wang, N. Mao, B. B. Huang, Y. Mokrousov, and Y. Dai, Antiferromagnetic topological insulator with nonsymmetric protection in two dimensions, *Phys. Rev. Lett.* **124**, 066401 (2020).
- [46] X. R. Zou, R. H. Li, Z. Q. Chen, Y. Dai, B. B. Huang, and C. W. Niu, Engineering gapless edge states from antiferromagnetic Chern homobilayer, *Nano. Lett.* **24**, 450 (2023).
- [47] See Supplemental Material at <http://link.aps.org/supplemental/10.1103/PhysRevB.109.174405> for which demonstrates the crystal structure, Berry curvature, surface states, etc., to help deepen readers' understanding of the article.